Current Optics and Photonics
Vol. 4, No. 4, August 2020, pp. 277-285

ISSN: 2508-7266(Print) / ISSN: 2508-7274(Online)
DOI: https://doi.org/10.3807/COPP.2020.4.4.277

An Evaluation Model for Analyzing the Overlay Error of Computer-generated Holograms

Zihao Gan[1], Xiaoqiang Peng[1,2]*, and Huajie Hong[1]

[1]College of Intelligence Science, National University of Defense Technology, Changsha 410073, China
[2]Laboratory of Science and Technology on Integrated Logistics Support, National University of Defense Technology, Changsha 410073, China

(Received April 21, 2020 : revised June 1, 2020 : accepted June 23, 2020)

Computer-generated holograms (CGH) are the core devices to solve the problem of freeform surface measurement. In view of the overlay error introduced in the manufacturing process of CGH, this paper proposes an evaluation model for analyzing the overlay error of CGH. The detection method of extracting CGH profile information by an ultra-depth of field micro-measurement system is presented. Furthermore, based on the detection method and technical scheme, the effect of overlay error on the wavefront accuracy of CGH can be evaluated.

Keywords : Computer-generated holograms, Overlay error, Evaluation model, Wavefront accuracy
OCIS codes : (050.1380) Binary optics; (090.1760) Computer holography; (090.1970) Diffractive optics; (120.4630) Optical inspection

I. INTRODUCTION

The freeform surface has the ability to balance the full-field aberration of an optical system, which can meet the requirements of high performance, lightweight and miniaturization. Therefore, it has become more and more important in the field of modern optical engineering [1-3]. With the development of the freeform surface, its surface testing technology has gradually become a key factor restricting the manufacturing precision of such optical parts [4]. Because CGH can generate reference wavefront of any shape based on diffraction theory [5-7], it compensates for various types of aberrations and has become a core device for solving the problem of freeform surface tests.

For CGH elements, the pattern of the master hologram for testing the shape of the surface is usually phase-type fringes [8]. In order to realize the precise positioning of the CGH itself, it is usually necessary to make an alignment hologram on the substrate of the master hologram at the same time. The pattern of the alignment hologram adopts amplitude-type fringes, with 3rd-order reflected light as the reference wavefront [9]. Due to the difference in the fabrication process between the two types of CGH, it needs to go through two direct writing processes [10, 11]. Figure 1 shows the process flow for making a complex-type CGH pattern. Generally, laser direct writing or electron beam direct writing is used for exposure [12, 13]. Introducing overlay error during the two previous exposures is inevitable, leading to the deviation of alignment hologram and master hologram. This error would affect the measurement results of the surface shape [14].

For the overlay error introduced in the manufacturing process of complex-type CGH, no related literature reports have been published to evaluate or calibrate such error. This paper focuses on this problem and proposes an evaluation method based on image feature recognition. The content can be applied to calibrate the influence of holographic pattern deviation on the surface measurement results, so as to effectively improve the testing accuracy of freeform surface by CGH.

II. EXPERIMENTAL SETUP

The ultra-depth of field microscope has the advantages of large depth of field, high resolution, and real-time shooting,

*Corresponding author: pengxiaoqiang@nudt.edu.cn, ORCID 0000-0001-9476-8026
Color versions of one or more of the figures in this paper are available online.

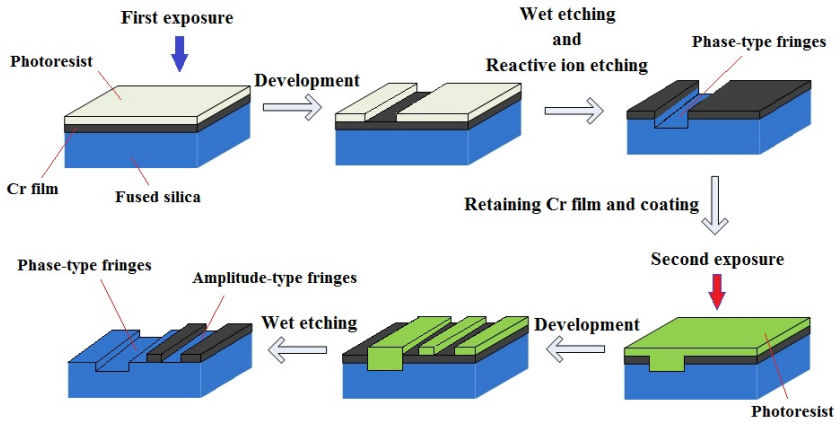

FIG. 1. The process flow for making a complex-type CGH.

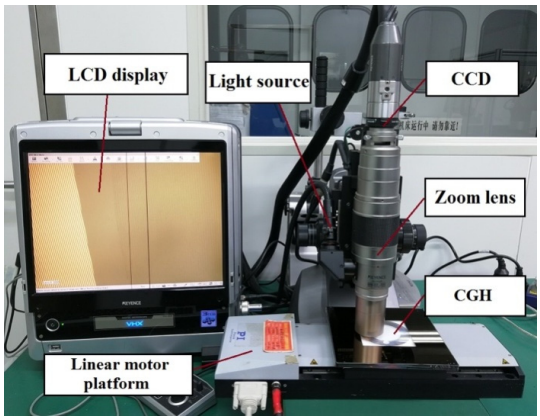

FIG. 2. Physical setup of error calibration system.

so it can be used to characterize the pattern information of CGH fringes.

We use a high-definition zoom lens that can achieve continuous shooting at a magnification of 500 to 5000, and high contrast fringe images can be obtained by adjusting the depth of field. Figure 2 shows a system for calibrating CGH pattern error, the system is mainly composed of a measurement device, mechanical transmission and control part. The measurement device is an image shooting device modified by VHX-6000 ultra-depth of field microscope, including lighting source, high-resolution zoom lens, CCD camera and liquid crystal display (LCD). The mechanical transmission part adopts the electric control platform of model M-511.DD. with positioning accuracy of 0.1 μm and straightness of 0.2 μm. The control part includes industrial computer and motion controller.

III. PRINCIPLE AND METHOD

3.1. CGH Profile Detection

The phase-type fringes of CGH can be characterized by the calibration system shown in Fig. 2. The specific steps can be expressed as

1) Select the target area to record its holographic pattern with calibration system, and import the images into MATLAB for grayscale processing. Figure 3 shows the measurement result and gray image of a local phase-type CGH.

2) Extract the fringe contour information. Figure 4(a) shows the grayscale distribution of the cross-section part from the original gray image, which needs to be filtered. For a certain image f (x, y), a threshold value T is set. After filtering, the grayscale value of the image is

$$g(x,y)=\begin{cases} NaN, f(x,y)>T \\ f(x,y), f(x,y)\le T \end{cases}, \tag{1}$$

where NaN stands for removing the data at that point, and the gradient of gray image f (x, y) at any position is a vector corresponding to the first derivative in the X and Y directions. Figure 4(b) shows the grayscale value of the pixels after the data of Fig. 4(a) is filtered. From the processed data, there will be a grayscale mutation in the local image, that is, the image edges [15]. The edge of the image can reflect the contour information of CGH fringes. The grayscale of edge features in the image shows a trend of decreasing first and then increasing, and there are obvious minimum points. We take the minimum points of edge features as the fringe contour to analyze, and the correctness of this setting will be verified by later experiments.

Since the digital image is discrete, the following formula can be used to calculate the partial derivative of a point f (x_i, y_j):

$$\begin{cases} G_x = f(x_i+1, y_i) - f(x_i, y_i) \\ G_y = f(x_i, y_i+1) - f(x_i, y_i) \end{cases}. \tag{2}$$

For a grayscale image of a holographic fringe, the grayscale changes dramatically at the fringe edge, and its first derivative distribution in one-dimensional direction is shown in Fig. 5(a). The different signs of the first derivative at both ends of the fringe edge (such as measurement points A

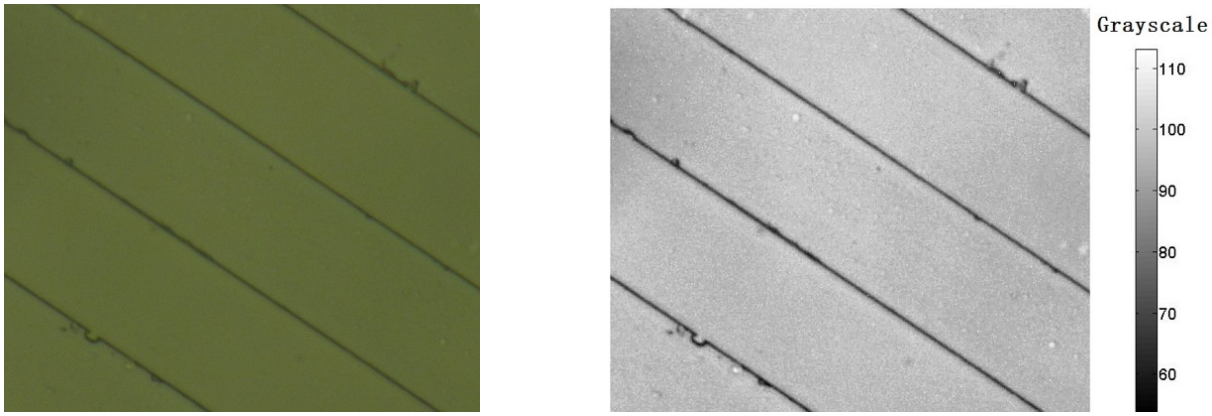

(a) Captured image (b) Grayscale image

FIG. 3. The measurement image of phase-type CGH.

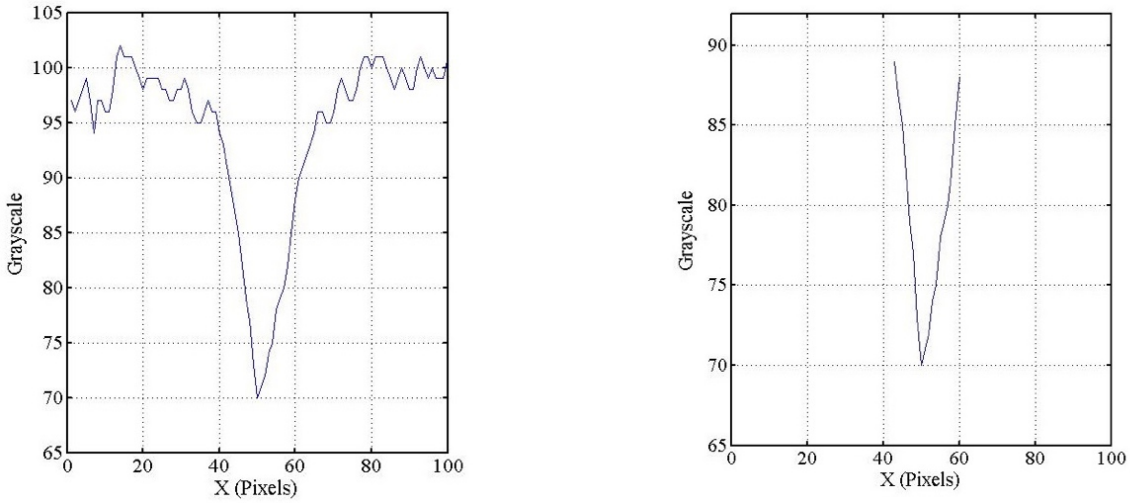

(a) Before filtering (b) After filtering

FIG. 4. Grayscale of each pixel on the image cross section.

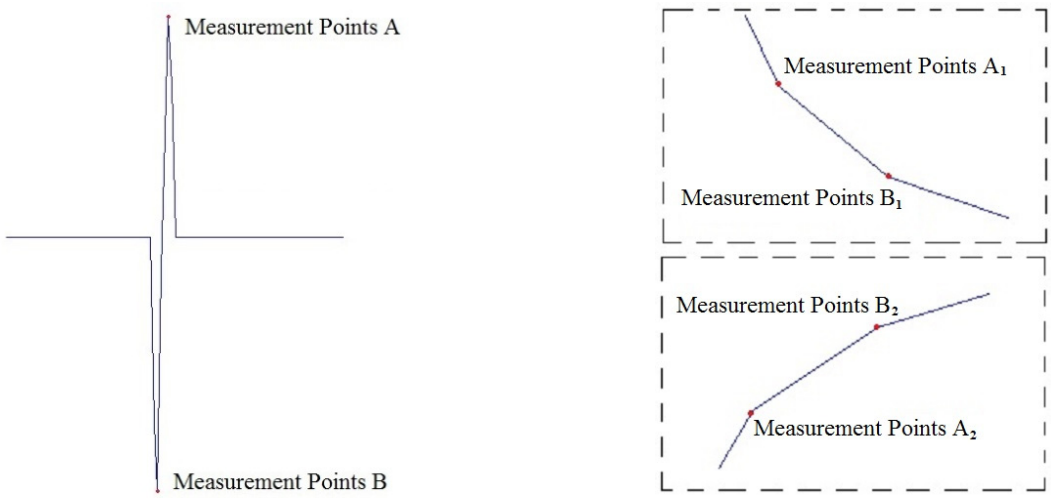

(a) Edge part (b) Non-edge part

FIG. 5. Schematic diagram of first derivative distribution.

and B in the figure). The distribution characteristics of the first derivative at the non-edge part are shown in Fig. 5(b). The numerical value changes smoothly, and there is no different sign of the first derivative at adjacent pixel points.

For the G_X distribution of grayscale image, the fringe edge points are searched row by row in the X direction, and the qualification conditions are as follows:

$$G_x(x_i, y_i) \cdot G_x(x_i + 1, y_i) \le 0 . \quad (3)$$

Among the points (x_i, y_j) and ($x_i + 1$, y_j), the point with the smaller G_x amplitude is taken as the fringe edge point. Similarly, the corresponding fringe edge points are obtained by searching in the Y direction according to the G_y distribution. Combining the two extracted data points, we can get the position information of fringe contour in the image.

The experimental device shown in Fig. 2 was exploited to characterize the amplitude pattern information. Figure 6(a) shows the grayscale processing results of the amplitude-type CGH. In the figure, the dark-colored area is fused silica with the chromium layer removed, while the bright-colored area is the part with the chromium layer retained. Figure 6(b) shows the grayscale value distribution of a group of cross-section data, and d is the average grayscale difference between the bottom and top of the groove. The contour information of CGH can be obtained by taking the position with the grayscale difference of d/2 as the fringe contour condition.

3.2. Evaluation Method

As shown in Fig. 7, the master hologram is a circular region, while the alignment hologram is a ring zone. According to the design CGH pattern, the center of the circle region (master hologram) coincides with the center of the ring region (alignment hologram), and the distance from the pattern node on the boundary of alignment hologram (the innermost or outermost ring) to the center of the circle is equal. Take the phase-type pattern as the measurement datum, the overlay error of the CGH can be obtained by detecting the deviation of the actual coordinates of the amplitude-type pattern from the design position.

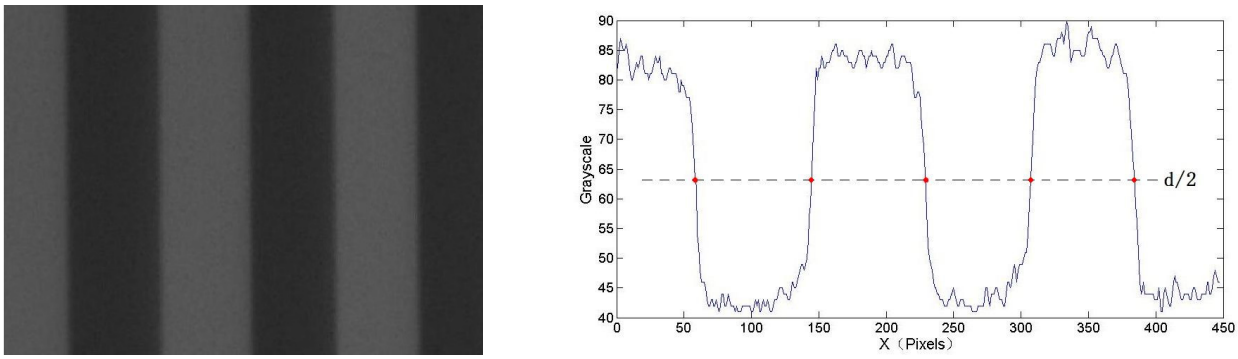

(a) Grayscale processing results (b) Grayscale distribution in the cross section

FIG. 6. The measurement image of amplitude-type CGH.

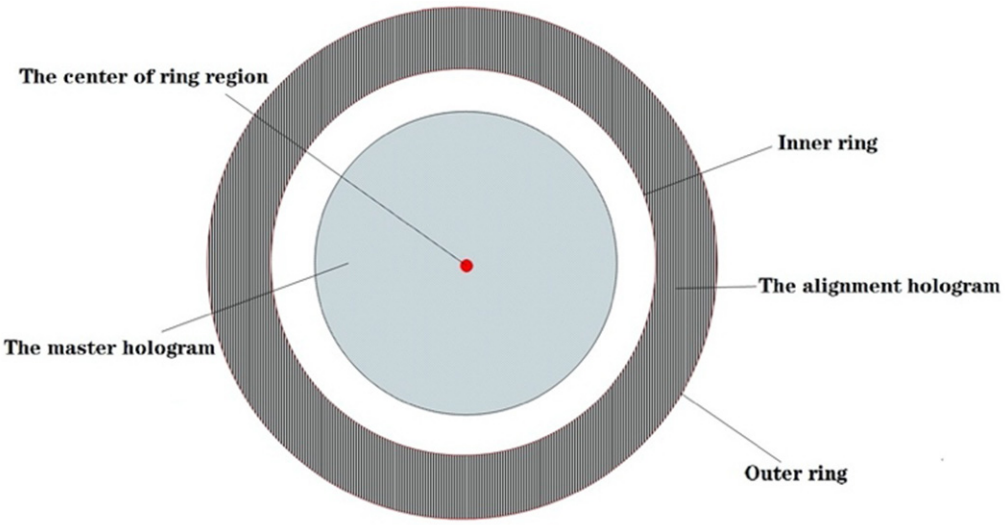

FIG. 7. The regional layout of complex-type CGH.

The pattern overlay error is characterized by an ultra-depth of field micro-measurement system, and the evaluation result of the error is calculated by simulation software. The specific methods are as follows:

1) Place the imaging lens on a certain feature pattern (recognizable characteristic fringe) of the master hologram, and take a set of image data with a super-depth of field microscope. Record the two-dimensional coordinates of the platform, and set several nodes of the feature pattern as datum points. The position of the datum point in the measurement coordinate system is calculated by the image processing method as (x^m, y^m), and the position of the datum point in the encoding coordinate system [7] is (x^d, y^d), The two types of coordinate values meet matching relationship

$$\begin{cases} x^d = x^m \times \cos\theta + y^m \times \sin\theta + c \\ y^d = -x^m \times \sin\theta + y^m \times \cos\theta + h \end{cases}, \tag{4}$$

where θ is the rotation angle; c is the shift quantum in the X direction; h is the shift quantum in the Y direction. By substituting the coordinate value into Eq. (4), the pose transformation matrix B (θ, c, h) of the measurement coordinate system corresponding to the encoding coordinate system can be obtained by iterative least square method.

2) Take the nodes on the edge of the alignment hologram ring (usually the inner or outer ring) as the testing object. Based on the real-time observation function of a microscope, several groups of images including the node information are taken at different positions by the platform movement, and the displacement values of a platform are recorded. The positions of nodes (X_1, Y_1), (X_2, Y_2) and (X_3, Y_3) in the encoding coordinates can be calculated by combining the image processing method and the pose transformation matrix B.

3) According to the positions of three nodes on the edge of the alignment hologram ring, the center coordinate of the real region can be obtained. Compared with the center coordinate of the ideal ring zone, the relative position deviation ΔX and ΔY (the dislocation value of CGH relative to the optical axis in surface test) can be obtained.

4) The relative position deviation is imported into the CGH testing path of ZEMAX software, and the distribution diagram of wavefront error introduced by the overlay error can be obtained through simulation calculation.

IV. RESULT ANALYSIS

4.1. Verification of Contour Detection Algorithm

To verify the accuracy of the contour detection algorithm based on image processing, we conducted the following experiments.

In the process of characterizing the master hologram pattern with the measurement system, the CGH contour detection algorithm based on image processing needs to be verified. The local phase grating was selected as the experimental object. The grating pattern was recorded under a 3000X lens with the micro measurement system, as shown in Fig. 8(a). Since the overall direction of the fringe is X direction, we only need to extract the fringe edge points based on the first derivative distribution in the Y direction. Based on the aforementioned detection method to process the measurement results, the position of image edge points can be calculated, as shown in Fig. 8(b) (the set of white points in the figure is image edge data).

Although there may be a small amount of noise in the image results, it does not affect the effective acquisition of the CGH contour information. Because the characterization part is a straight fringe structure, the contour information can be obtained through several edge points. The three groups of fringe periods can be calculated as 7.510 μm (126.0 pixels), 7.569 μm (127.0 pixels) and 7.629 μm (128.0 pixels). Figure 9 shows the design pattern corresponding to the local grating area, and the standard period of the three groups of gratings are 7.659 μm, 7.685 μm and 7.684 μm, respectively.

We exploited Atomic Force Microscopy (AFM) to characterize the size of these three groups of fringes, and the

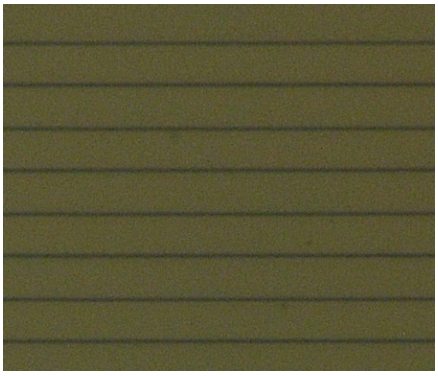

(a) Captured image

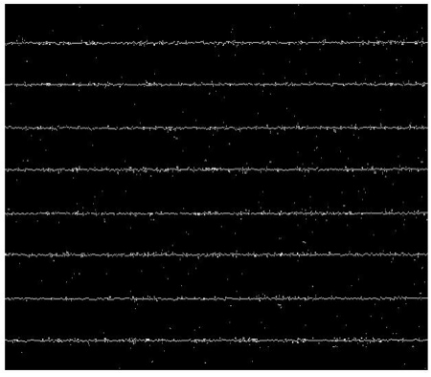

(b) Edge detection point

FIG. 8. Processing results of grating detection data.

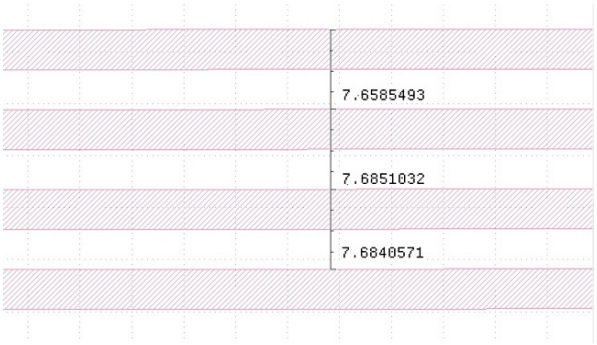

FIG. 9. The design pattern of local grating.

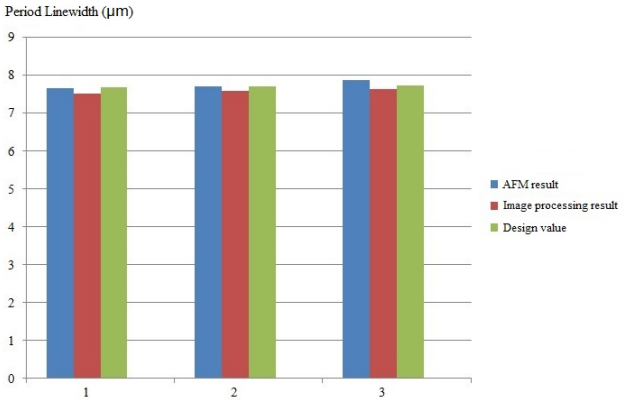

FIG. 10. The linewidth results of fringe periods by different way.

period linewidth was 7.683 μm, 7.703 μm and 7.722 μm, respectively. Figure 10 shows the linewidth results of three groups of fringe periods based on design, image processing and AFM measurement. The result deviation between the image edge detection and the AFM measurement is 1.73%, and the deviation between the image edge detection and the design value is 1.39%. Therefore, these results verified the accuracy of the image detection algorithm.

4.2. Application

According to the application requirements of an optical system, we use a freeform mirror with non-rotational symmetry, and its surface expression is as follows:

$$z(x,y)=\frac{m(x^2+y^2)}{1+\sqrt{1-(1+k)(x^2+y^2)}}+A_1x+A_2y+B_1x^2+B_2xy+B_3y^2 +C_1x^3+C_2x^2y+C_3xy^2+C_4y^3 +D_1x^4+D_2x^3y+D_3x^2y^2+D_4xy^3+D_5y^4. \quad (5)$$

In order to meet the demand of the surface measurement, we made a corresponding CGH element, and analyzed the CGH sample as an example. Figure 11(a) shows the layout of CGH optical test system, and Fig. 11(b) represents the residual aberration results of CGH design.

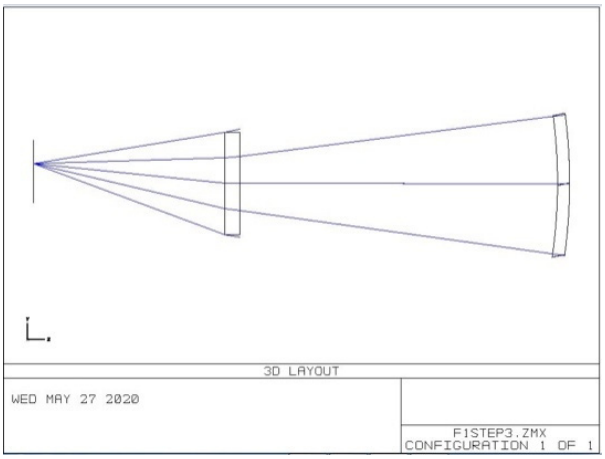

(a) The layout of optical test system

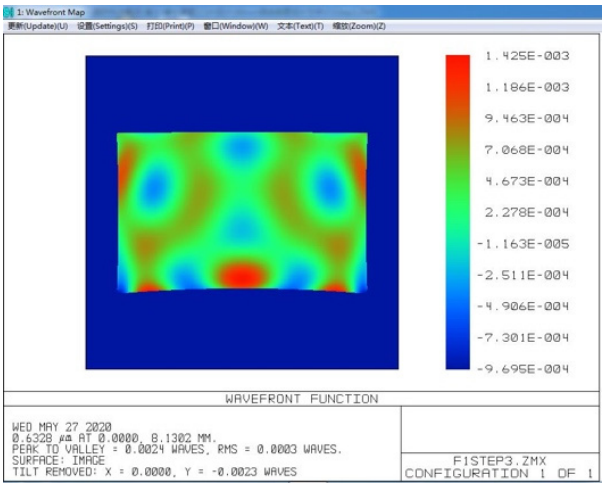

(b) The residual aberration

FIG. 11. CGH design results.

We exploited the device system shown in Fig. 2 to detect the overlay error of CGH. On the one hand, the straightness and flatness of the control platform can reach 0.2 μm. On the other hand, the substrate used to fabricate the CGH pattern is a quartz plane plate. According to the factory specification, its surface precision PV value is within 0.1 μm. Based on the above two factors, it can be seen that errors due to height (z-axis) can be ignored in the process of platform movement.

We measured the first set of characteristic patterns by an ultra-depth of field microscope in the master hologram area, as shown in Fig. 12(a). Set point A_1 and point B_1 in the figure as reference points of the master hologram, and record the platform coordinate as 28.71 mm. The platform was moved to the edge of the alignment hologram ring and a set of holographic patterns was measured, as shown in Fig. 12(b). Point C_1 in the figure is the node on the inner ring band, and the platform coordinate is recorded as 28.85 mm. Based on the feature point matching method, the coordinate value of the point C_1 was calculated as (-1.7185 mm, -22.0309 mm).

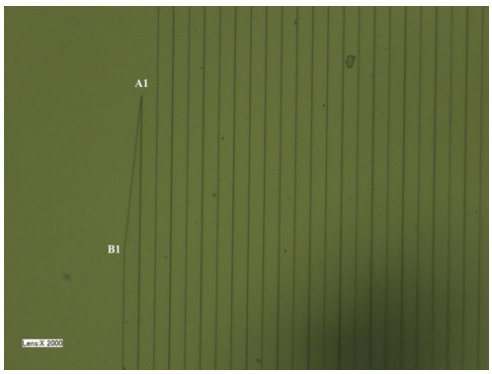

(a) Feature pattern on the master hologram

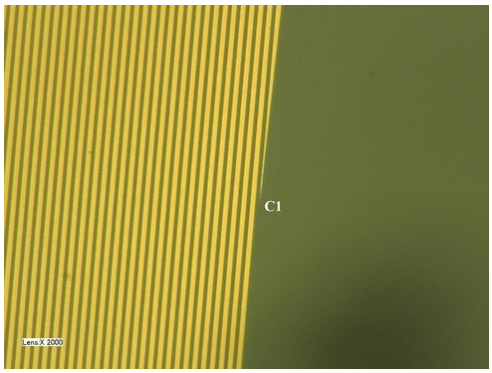

(b) Ring band of the alignment hologram

FIG. 12. The first group of measurement results.

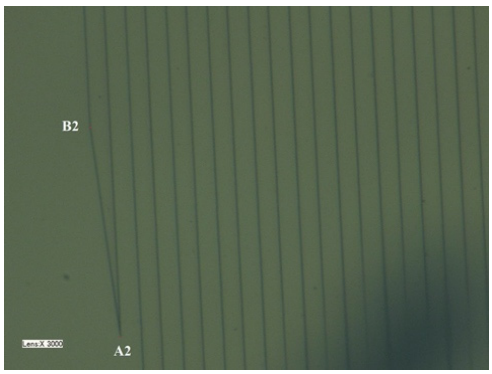

(a) Feature pattern on the master hologram

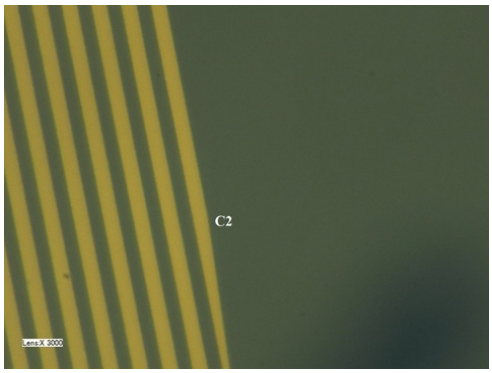

(b) Ring band of the alignment hologram

FIG. 13. The second group of measurement results.

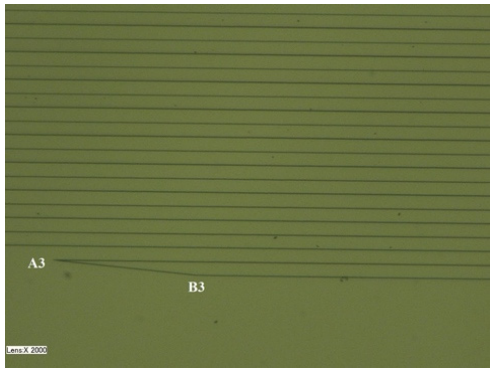

(a) Feature pattern on the master hologram

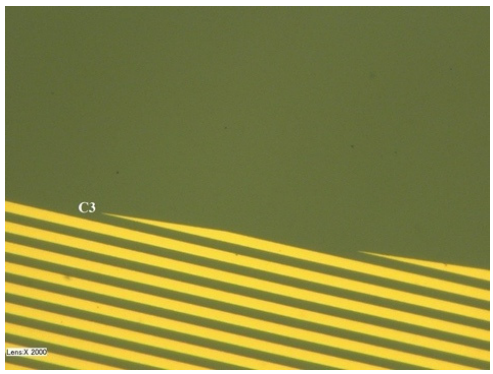

(b) Ring band of the alignment hologram

FIG. 14. The third group of measurement results.

The second set of feature patterns was measured in the master hologram area, as shown in Fig. 13(a). Set point A_2 and point B_2 in the figure as reference points of the master hologram, and record the platform coordinate as 33.3 mm. The point C_2 in Fig. 13(b) is a node on the inner ring band of the alignment hologram, and the one-dimensional platform coordinate is recorded as 33.42 mm. The coordinate value of the point C_2 was calculated as (-1.5932 mm, 22.0411 mm).

The third set of feature patterns was measured in the master hologram area, as shown in Fig. 14(a). Set point A_3 and point B_3 in the figure as reference points of the master hologram, and record the platform coordinate as 11.5 mm. The point C_3 in Fig. 14(b) is a node on the inner ring band of the alignment hologram, and the one-dimensional platform coordinate is recorded as 12.45 mm. The coordinate value of the point C_3 was calculated as (2.5578 mm, 21.9514 mm).

According to the position of three nodes on the alignment hologram ring, the real coordinate of manufacturing center can be calculated as (7.191 μm, 0.372 μm). However, the ideal central coordinate of the ring is (0,0), so the relative position deviation: ΔX = 7.191 μm; ΔY = 0.372 μm. By substituting the deviation into the CGH test optical path in ZEMAX, the residual wavefront aberrations influenced by overlay error was simulated as shown in Fig. 15. It can be seen from Fig.

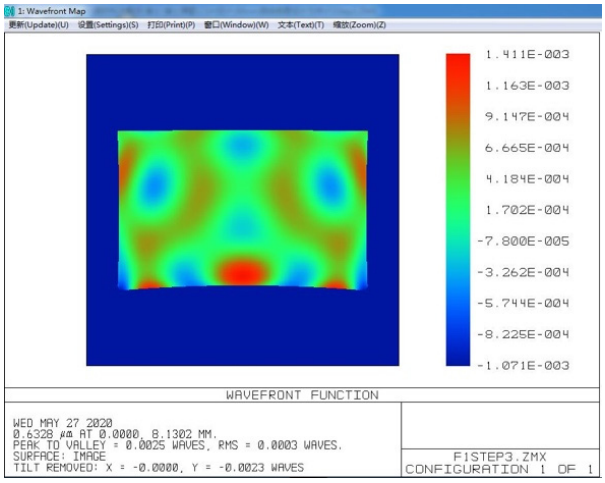

FIG. 15. The residual wavefront aberrations influenced by overlay error.

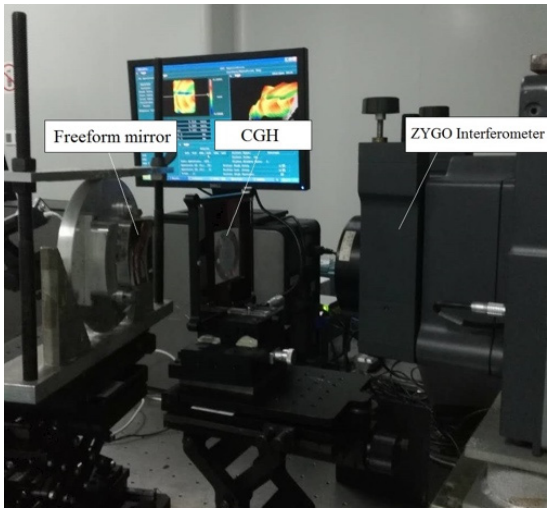

(a) Physical setup of optical path structure

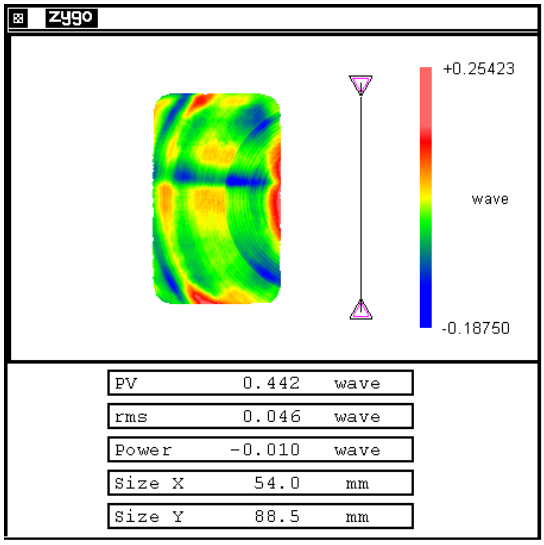

(b) Surface measurement results

FIG. 16. The experiment of freeform surface test by CGH.

11(b) and Fig. 15 that both wavefront errors are 0.0003λ (RMS). Therefore, it can be considered that the overlay precision of the CGH sample is up to quality standard.

We used the calibration results of the CGH sample to guide the actual machining process. The surface shape error of the freeform mirror was tested by the CGH sample, and the optical path structure is shown in Fig. 16(a). Based on the surface error obtained by each measurement, the freeform surface was repeatedly polished. During the processing, the testing results of the CGH displayed an obvious convergence feature, and the final results of surface error were shown in Fig. 16(b).

V. CONCLUSION

The article proposed an analysis model for evaluating the CGH overlay error based on the micro-measurement system. The specific contents include: 1) A data processing algorithm for extracting CGH contour information from microscopic images; 2) The technical scheme of calibrating the CGH wavefront error introduced by the overlaying process. The contour detection method was verified by design experiment. Taking the CGH sample for freeform surface test as the testing objective, the error evaluation of sample was completed by the evaluation method. The results can provide an important basis for strict control of CGH manufacturing quality.

ACKNOWLEDGMENT

This work is supported by the Science Challenging Program (TZ2018006) and Young Teacher Innovation Research Project (ZN2019-5).

REFERENCES

1. K. P. Thompson and J. P. Rolland, "Freeform optical surfaces: a revolution in imaging optical design," Opt. Photon. News **23**, 30-35 (2012).
2. Z. Feng, B. D. Froese, C.-Y. Huang, D. Ma, and R. Liang, "Creating unconventional geometric beams with large depth of field using double freeform-surface optics," Appl. Opt. **54**, 6277-6281 (2015).
3. P. J. Smilie and T. J. Suleski, "Variable-diameter refractive beam shaping with freeform optical surfaces," Opt. Lett. **36**, 4170-4172 (2011).
4. Y. Xie, X. Mao, J. Li, F. Wang, P. Wang, R. Gao, X. Li, S. Ren, Z. Xu, and R. Dong, "Optical design and fabrication of an all-aluminum unobscured two-mirror freeform imaging telescope," Appl. Opt. **59**, 833-840 (2020).
5. Z. Pang, Z. Ma, X. Fan, and G. Zou, "Design and fabrication of CGH for 600 mm diameter SiC primary mirror surface figure testing," Proc. SPIE **9684**, 96842J (2016).

6. A. G. Poleshchyk and R. K. Nasyrov, "High-precision aspherical wavefront shaping with combined computer generated holograms," Proc. SPIE **8759**, 875929 (2013).
7. Z.-H. Gan, X.-Q. Peng, S.-Y. Chen, C.-L. Guan, H. Hu, X.-L. L, and Z.-C. Dai, "Fringe discretization and manufacturing analysis of a computer-generated hologram in a null test of the freeform surface," Appl. Opt. **57**, 9913-9921 (2018).
8. P. Su, J. Ma, Q. Tan, G. Kang, and Y. Liu, "Computer generated hologram null test of a freeform optical surface with rectangular aperture," Opt. Eng. **51**, 025801 (2012).
9. R. Zehnder, J. H. Burge, and C. Zhao, "Use of computer generated holograms for alignment of complex null correctors," Proc. SPIE **6273**, 62732S (2006).
10. H.-G. Rhee and Y.-W. Lee, "Improvement of linewidth in laser beam lithographed computer generated hologram," Opt. Express **18**, 1734-1740 (2010).
11. S. M. Arnold, "Electron beam fabrication of computer-generated holograms," Opt. Eng. **24**, 245803 (1985).
12. H. Shen, R. Zhu, Z. Gao, E. Y. B. Pun, W. H. Wong, and X. Zhu, "Design and fabrication of computer-generated holograms for testing optical freeform surfaces," Chin. Opt. Lett. **11**, 032201 (2013).
13. A. G. Poleshchuk, V. P. Korolkov, R. K. Nasyrov, and J. M. Asfour, "Computer generated holograms: fabrication and application for precision optical testing," Proc. SPIE **7102**, 710206 (2008).
14. J. Feng, C. Deng, and T. Xing, "Design and error analysis of the computer-generated hologram used for concave aspheric surface testing," Laser Optoelectron. Prog. **49**, 110902 (2012).
15. R. Maini and H. Aggarwal, "Study and comparison of various image edge detection techniques," Int. J. Image process. **3**, 1-11 (2009).